






The impact of astrophysical priors on parameter inference for GW230529

Debatri Chattopadhyay ^{*}, Sama Al-Shammari ^{*}, Fabio Antonini ^{*}, Stephen Fairhurst ^{*},
Benjamin Miles and Vivien Raymond ^{*}

School of Physics and Astronomy, Cardiff University, Cardiff CF24 3AA, UK

Accepted 2024 October 14. Received 2024 October 9; in original form 2024 July 11

ABSTRACT

We investigate the effects of prior selection on the inferred mass and spin parameters of the neutron star–black hole merger GW230529_181500. Specifically, we explore models motivated by astrophysical considerations, including massive binary and pulsar evolution. We examine mass and spin distributions of neutron stars constrained by radio pulsar observations, alongside black hole spin observations from previous gravitational-wave detections. We show that the inferred mass distribution highly depends upon the spin prior. Specifically, under the most restrictive, binary stellar evolution models, we obtain narrower distributions of masses with a black hole mass of $4.3^{+0.1}_{-0.1} M_{\odot}$ and neutron star mass of $1.3^{+0.03}_{-0.03} M_{\odot}$ where, somewhat surprisingly, it is the prior on component spins that has the greatest impact on the inferred mass distributions. Re-weighting using neutron star mass and spin priors from observations of radio pulsars, with black hole spins from observations of gravitational waves, yields the black hole and the neutron star masses to be $3.8^{+0.5}_{-0.6} M_{\odot}$ and $1.4^{+0.2}_{-0.1} M_{\odot}$, respectively. The sequence of compact object formation – whether the neutron star or the black hole formed first – cannot be determined at the observed signal-to-noise ratio. However, there is no evidence that the black hole was tidally spun up.

Key words: gravitational waves.

1 INTRODUCTION

The gravitational-wave (GW) event GW230529_181500 (hereafter abbreviated GW230529) was detected by the LIGO Livingston Observatory during the first part of the fourth observing run of the LIGO (Laser Interferometer Gravitational-Wave Observatory)–Virgo–KAGRA (LVK) collaboration (Abac et al. 2024). The binary components are a neutron star (NS) and another compact object whose mass likely falls within the ‘lower mass gap’ between the heaviest NSs and the lightest black holes (BHs), which was previously thought to exist between 2.5 and $\sim 5 M_{\odot}$ (Bailyn et al. 1998; Özel et al. 2010; Farr et al. 2011). Moreover, the event marks the third confident detection of a BH–NS (BHNS) binary through GWs (Abbott et al. 2021). It followed a probable observation of a pulsar–mass gap BH in the globular cluster (GC) NGC 1851 (Barr et al. 2024). Theoretical astrophysics of massive binary evolution has speculated about the existence of BHNS binaries (O’Shaughnessy et al. 2008; Fryer et al. 2012; Broekgaarden et al. 2021; Chattopadhyay et al. 2021). Still, successive detections of such objects spark more debates on their mass–spin distributions to formation channels (Chandra et al. 2024) to possible electromagnetic counterparts (Ronchini et al. 2024; Zhu et al. 2024).

The detection of GW230529 has significant implications for our understanding of stellar evolution and the end stages of massive stars, since it might provide further evidence for compact objects existing within the mass gap (Zevin et al. 2020; Siegel et al. 2023; Martineau et al. 2024; Zhu et al. 2024). In the pre-GW era, this

perceived mass gap led theoreticians to speculate on the supernova mechanisms. For example, the rapid and delayed supernova models discussed in Fryer et al. (2012) present different growth time-scales for the instabilities driving the explosion of massive stars. The rapid supernova model can reproduce the mass gap, suggesting that the formation of NSs and BHs occurs within distinct mass ranges. In contrast, the delayed supernova model, where supernova explosions occur long after the bounce shock, predicts that the mass gap will be populated. The delayed model will therefore imply a smoother transition in the remnant masses of supernovae and allow for the existence of compact objects with masses in the gap (Belczynski et al. 2012; Olejak et al. 2022).

The inherent limitations in recovering the binary physical parameters from the GW data hinder the accurate measurement of the component masses and spin parameters in a GW event such as GW230529. While the component masses and spins are the most (astro)physically interesting quantities, they are not the variables that most directly affect the emitted GW. Those are the chirp mass \mathcal{M} , mass ratio q , and effective spin χ_{eff} (which we define in Section 2). For a low-mass system such as GW230529, the chirp mass is measured with good accuracy, with $\mathcal{M} = 1.94 \pm 0.04 M_{\odot}$, while there is significantly larger uncertainty on the mass ratio and effective spins (Abac et al. 2024). Furthermore, as is well known (Cutler & Flanagan 1994; Hannam et al. 2013), there is a degeneracy between the measured mass ratio values and effective spin. Consequently, changing the prior assumptions for spins of the binary component can significantly impact the inferred mass distributions and, conversely, changing the mass assumptions can impact the inferred spins. In this work, we investigate the impact of using astrophysically motivated

* E-mail: ChattopadhyayD@cardiff.ac.uk

distributions for the masses and spins of BHs and NSs on the inferences about the progenitor properties of GW230529.

The remainder of the letter is laid out as follows: in Section 2, we briefly summarize the methods used to incorporate astrophysical priors; in Section 3, we introduce the astrophysical observations and models used; in Section 4, we present the results; and we conclude in Section 5 with a discussion and possible future directions.

2 INCORPORATING ASTROPHYSICAL PRIOR BELIEFS

The frequency evolution of a GW emitted by an inspiralling compact binary is determined, at leading order, by the chirp mass, \mathcal{M} , of the system, while the mass ratio q , and effective spin, χ_{eff} , affect the signal at sub-leading orders (Blanchet 2006).¹ These quantities are related to the component masses ($m_{1,2}$) and spins ($S_{1,2}$):

$$\mathcal{M} = \frac{(m_1 m_2)^{3/5}}{(m_1 + m_2)^{1/5}}, \quad (1)$$

$$q = \frac{m_2}{m_1}, \quad (2)$$

$$\chi_{\text{eff}} = \frac{(m_1 \chi_1 + m_2 \chi_2) \cdot \hat{\mathbf{L}}}{m_1 + m_2}, \quad (3)$$

where $\hat{\mathbf{L}}$ is the unit vector in the direction of the orbital angular momentum, the spin, χ_i , is defined as $\chi_i = S_i/m_i^2$, and the normalization is chosen such that a maximally spinning BH has $|\chi| = 1$. Consequently, the inferred values of the component masses and spins from a GW observation correlate. Furthermore, the choice of priors can impact the inferred properties for a low signal-to-noise ratio (SNR) signal such as GW230529. Indeed, due to correlations between the inferred mass ratio and effective spin, choices of spin priors can impact the inferred masses and vice versa.

The GW estimation of these parameters for GW230529, as presented in Abac et al. (2024), was performed with minimally informed priors on the mass and spin distributions of the components of the binary, in addition to the location and orientation parameters (Veitch et al. 2015). Specifically, the analysis used mass priors that are flat in the redshifted component masses, within a prescribed range of masses and mass ratios, and uniform in spin magnitude and orientation (see appendix D of Abac et al. 2024 for details). The output of the original analysis is a set of samples from the posterior probability distribution of the parameters (LIGO Scientific Collaboration, Virgo Collaboration & KAGRA Collaboration 2024).² We then apply weights to these samples in the ratio of our desired *astrophysical* before the *original*, uniform prior. Given an astrophysically motivated prior π_A , the posterior distribution for the parameters θ describing the progenitor of GW230529 is given by

$$p_A(\theta|d) = \frac{\pi_A(\theta)p(d|\theta)}{p_A(d)}, \quad (4)$$

¹The precessing spin, χ_p , also impacts the observed waveform. However, as there is no evidence for precession in this observation and the in-plane spins are essentially unconstrained (see fig. 13 of Abac et al. 2024), we do not consider the precessing spin here.

²Specifically, we make use of the `Combined_PHM_highSpin` results for the majority of our analyses. When re-weighting using the astrophysical models described in Section 3.1, which restrict component spins to be close to zero, we use `IMRPhenomPv2_NRTidalv2_lowSpin` to ensure that we have sufficient samples following re-weighting.

where $p(d|\theta)$ is the likelihood of the data given the parameters θ . The denominator, $p_A(d)$, is the evidence that serves as an overall normalization of the distribution.

While it is possible to calculate this posterior directly from the data, it is more straightforward to *re-weight* the existing results obtained with the original, uninformed prior π_0 (see Payne, Talbot & Thrane 2019 for a demonstration). In particular, we can simply re-weight the distribution to obtain the posterior associated with the astrophysical prior:

$$p_A(\theta|d) = \frac{\pi_A(\theta)}{\pi_0(\theta)} p_0(\theta|d). \quad (5)$$

The posterior distribution is provided as a set of discrete samples θ_i whose density in parameter space follows the posterior distribution, $p_0(\theta|d)$. Thus, to obtain samples associated with the astrophysical prior, we calculate a weighting factor for each sample,

$$w_i = \frac{\pi_A(\theta_i)}{\pi_0(\theta_i)}. \quad (6)$$

This set of weighted samples provides updated parameter estimates under astrophysically motivated prior assumptions. To obtain a discrete set of equally weighted samples, we perform importance sampling on the weighted samples. This re-weighting is performed using importance sampling (Goertzel, United States Atomic Energy Commission & Oak Ridge National Laboratory 1950; Liu 2004; Robert & Casella 2004). To do this, we calculate the maximum weight w_{max} across the samples and then keep each of the samples θ_i with a probability

$$p_i = \frac{w_i}{w_{\text{max}}}. \quad (7)$$

When performing prior re-weighting, however, it is important that the proposed prior provides support in the same part of the parameter space as the target prior, otherwise the re-weighting will be highly inefficient. Since the original priors are near-uniform in the parameters of interest and also cover a broad parameter range, the astrophysical priors generally comprise a subset of the original ranges. However, in cases where the astrophysical priors are sharply peaked, the re-weighting procedure summarized above can lead to a low number of samples in the astrophysical posterior. In our analyses, we ensured a minimum of 1000 effective samples (Kish 1995; Elvira, Martino & Robert 2018). For the results presented in Section 4, we use those samples to create one-dimensional kernel density estimators of the inferred masses and spins. As 90 per cent credible intervals are the relevant numbers for the scientific conclusions of this work, we checked via bootstrapping tests to what precision the one-dimensional credible intervals could be quoted, and used that precision.

The astrophysical models introduced in the next section provide informed distributions for a subset of the parameters of the binary. We have no reason to use an informative prior for the sky location or orientation of the binary, so we do not re-weight these parameters in any of our studies. We are, however, interested in re-weighting (a subset of) the mass and spin parameters. Since the original priors for the masses, spin magnitudes, and orientations are independent, we are free to perform the re-weighting procedure described above separately for each parameter, provided that our astrophysically motivated priors are also independent in these parameters. In all cases, only a subset of the parameters is re-weighted, while the others retain the original, uninformative priors. Then, the re-weighting factorizes as

$$w_i = \frac{\pi_A(\theta_1)\pi_A(\theta_2)\dots\pi_A(\theta_n)}{\pi_0(\theta_1)\pi_0(\theta_2)\dots\pi_0(\theta_n)}. \quad (8)$$

When re-weighting the masses, we introduce new prior distributions for either m_1 , m_2 or both. When re-weighting the spins, we use astrophysically motivated distributions for one or both of the spin magnitudes $|\chi_i|$, or both the magnitudes and orientation through their impact upon the z -component of the spin

$$\chi_z = \chi \cdot \hat{L}. \quad (9)$$

3 MODELS

The astrophysically motivated distributions of masses and spins that we use later to inform our prior expectations for GW230529 are split into four distinct classes:

(i) Binary population synthesis models. These models are guided by existing theoretical and observational constraints on binary stellar evolution to produce merging binaries comprising an NS and a BH.

(ii) Models informed by radio pulsar observations. We make use of the masses and spins of NSs observed as millisecond pulsars to restrict the prior distributions of the NS mass and spin. The BH mass and spin are left agnostic.

(iii) Models informed by GW observations. The number of NS–BH (NSBH) mergers observed before GW230529 was small, therefore the inferred population properties are only weakly constrained. We instead consider the inferred BH spin distribution from the observed binary BH (BBH) population (Abbott et al. 2023) as a prior for the BH spin in GW230529. The NS mass and spin are left agnostic.

(iv) Models informed by observations of NSs and BHs. Finally, as the second and third classes of models independently constrain the NS parameters and BH spins, we apply both constraints concurrently.

The different models are summarized in Table 1 and the relevant quantities are plotted in Fig. 1.

3.1 Models motivated by binary astrophysics

Binary stellar evolution models can be used to predict the mass and spin distributions of BHs and NSs in merging binaries. For this letter, we consider a set of astrophysical models generated using the population synthesis code COMPAS (Hurley, Pols & Tout 2000; Hurley, Tout & Pols 2002; Fryer et al. 2012; Stevenson et al. 2019; Riley et al. 2022). Our base is the fiducial model, described in Chattopadhyay et al. (2021) (see also Broekgaarden et al. 2021), expanded to explore variations in metallicity, binary evolution, and pulsar evolution assumptions. The details of the prescriptions used to model the pulsar spin-down due to magnetic breaking are outlined in Chattopadhyay et al. 2020 (section 2) and Chattopadhyay et al. 2021 (section 2.3).

In most situations (>90 percent), it is expected that the more massive compact object, namely the BH, will form first. However, for low-mass binaries with similar zero-age main-sequence masses, the slightly more massive initial star can transfer mass to its companion, causing a mass-ratio reversal. The primary star then can become an NS first, followed by the secondary forming a light BH (for solar metallicity, median around $3.8 M_\odot$, as shown in table 3 of Chattopadhyay et al. 2021, although extended tails). We consider a set of models consisting of the two sub-populations BHNS or NSBH to reflect on the order of formation of the compact objects – whether the BH is born first (BHNS) or the NS is born first (NSBH).

Our fiducial model has metallicity $Z = 0.02$; the common envelope parameter that sets the fraction of orbital energy capable of unbinding the envelope is $\alpha = 1$ (Xu & Li 2010; Ivanova et al. 2013);

we adopt the ‘optimistic’ scenario for common envelope evolution where a Hertzsprung gap donor can survive and eject the envelope (Belczynski et al. 2007); we consider the ‘delayed’ supernova prescription by Fryer et al. (2012); we set the magnetic field decay time-scale affecting both non-recycled and recycled pulsars, $\tau_d = 1000$ Myr (see equation 5 of Chattopadhyay et al. 2020); and we take the mass-decay time-scale $\Delta M_d = 0.2 M_\odot$, which only affects recycled pulsars (equation 12 of Chattopadhyay et al. 2020).

In the other six models, we change one assumption from the fiducial model. These changes are (i) metallicity $Z = 0.005$, (ii) common envelope $\alpha = 3.0$, (iii) ‘pessimistic’ common envelope prescription (Belczynski et al. 2007), (iv) ‘rapid’ supernova modelling (Fryer et al. 2012), (v) $\tau_d = 500$ Myr, ensuring a slower spin-down of both recycled and non-recycled pulsars, and (vi) $\Delta M_d = 0.02 M_\odot$. After testing all seven models (fiducial, and the six variations), we conclude that the effect on the inferred mass of the compact objects is negligibly small. Model (v) with $\tau_d = 500$ Myr shows the widest NS spin priors of all models and hence was chosen to represent the astrophysical model set, with the name ‘FDT500’ (identical to the original paper Chattopadhyay et al. 2021).

While the NS spin is computed in detail with spinning down (and up, through mass transfer) of pulsars, the BH spins are varied only in the NSBH sub-population under the assumption of tidal spin-up of the BH progenitor by the first-born compact object (NS, in our case). Due to efficient angular momentum transport from core to envelope in He-star progenitor BHs, BHs are expected usually to be born non-spinning; however, in the case of NSBHs where the BH is born second, tidal effects from the first-born compact object (NS in this case) can potentially spin the second-born BH up at birth (Qin et al. 2018; Bavera et al. 2020). Lower mass, high-spin BHs are also expected to be more efficient at generating electromagnetic counterparts at mergers with NSs (Barbieri et al. 2020). Therefore, we also consider a population of BHs that form with significant spin, calling it ‘FDT500.Q’. The spinning up of the BH is a function of the binary orbital period right before the second supernova and the metallicity of the binary (which determines the masses of the compact objects). The fits are derived from Qin et al. (2018) models and illustrated in equations (2) and (3) of Chattopadhyay et al. (2022).

In Fig. 1, we show the inferred distribution of the z -component of the spin, χ_z , for the NS and BH in the models discussed above. All spins are oriented with the orbital angular momentum, assuming efficient tidal alignments. However, the BH spin-up model FDT500.Q shows extremely high spins that are completely unsupported by the data and hence discarded. The non-spinning BH model of NSBHs is considered for prior choices, BHNSs always have non-spinning BHs.

3.2 Models motivated by radio pulsar observations in star clusters

As an alternative approach to modelling isolated binary evolution, here we utilize the observed population of Galactic GC radio millisecond pulsar³ spin distribution from the Australia Telescope

³Over a third of all observed millisecond pulsars appear in Galactic GCs, which collectively account for less than 0.05 percent of the total number of stars in the Milky Way. These millisecond pulsars have spins up to $\chi \simeq 0.4$, several times or even order(s) of magnitude lower than normal pulsars. Although NSBH mergers in star clusters are rare (Ye et al. 2020), and NSs spin down significantly over time before the merger, these high-spin pulsars suggest an alternative formation channel that merits exploration.

Table 1. The models we use for re-weighting, as described in detail in Section 3.

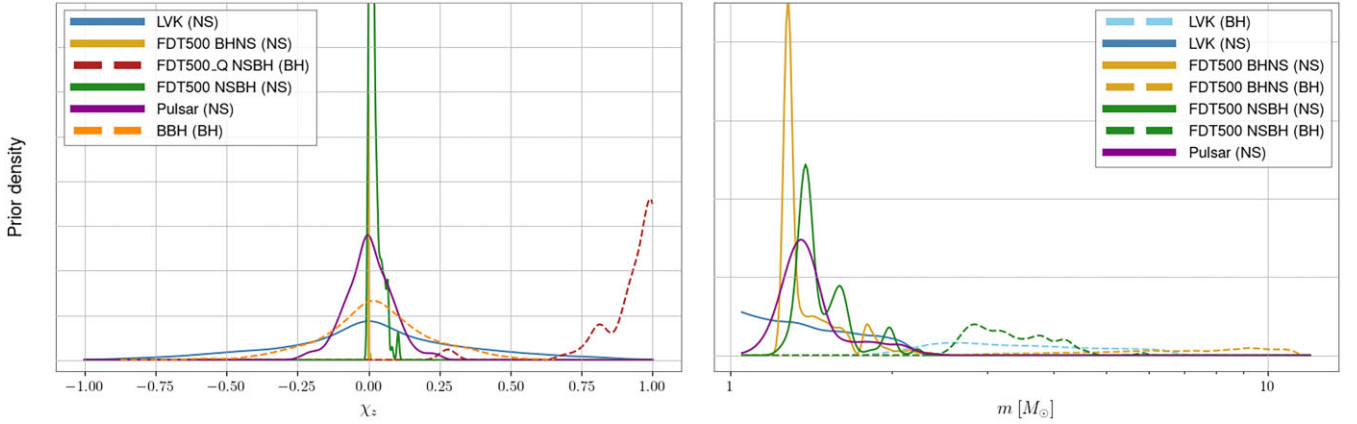
Model	Description	M_{BH}	M_{NS}	χ_{BH}	χ_{NS}	Tilt BH	Tilt NS
LVK	Uninformed priors ^a	Flat in det. frame ^a	Flat in det. frame ^a	Uniform [0–1]	Uniform [0–1]	Uniform	Uniform
FDT500	Astro. model ^b	Fit to model	Fit to model	≈ 0	$< 10^{-2}$	Aligned	Aligned
FDT500.Q	Astro. model with BH tidal spin-up ^c	Fit to model	Fit to model	Fit to model	$< 10^{-2}$	Aligned	Aligned
Pulsar	Pulsar mass + GC millisecond pulsar spin ^d	Uniform	Fit to pulsars	Uniform [0–1]	Fit to pulsars	Uniform	Uniform
BBH	BBH inferred mass, spin from GWTC-3 ^e	Uniform	Uniform	BBH χ	Uniform [0–1]	BBH tilt	Uniform
Pulsar + BBH	Pulsar mass, spin + GW BBH mass, spin	Uniform	Fit to pulsars	BBH χ	Fit to pulsars	BBH tilt	Uniform

^aIdentical to Abac et al. (2024) ‘primary combined analysis’.

^bFrom Chattopadhyay et al. (2021), $Z = 0.02$, common envelope optimistic, $\alpha = 1$, rapid supernovae, $\tau_d = 500$ Myr, and $\Delta M_d = 0.2 M_\odot$.

^cAs previous, with BH tidal spin-up (Qin et al. 2018).

^dObserved radio pulsar mass from Rocha et al. (2023); GC millisecond pulsar spins from ATNF catalogue.

^eFrom Abbott et al. (2023), BBH mass, spin distribution.

Figure 1. The prior distributions for the models outlined in Section 3: the astrophysical models (Section 3.1), the pulsar population models (Section 3.2), and the GW population models (Section 3.3), as well as the priors used by the LVK analysis. The left plot shows the distributions of the spin projected along the orbital angular momentum χ_z ; note that the astrophysical FDT500 BHNS models predict very small spins, while the astrophysical FDT500.Q NSBH models predict spins largely incompatible with GW230529. We used the FDT500 models as representative of our astrophysical re-weighting. The pulsar population distribution assumed uniform spin orientation. The right plot shows the mass distributions; note that we are not using the mass distributions from the BBH population model in the re-weighting.

National Facility (ATNF) pulsar catalogue⁴ (Manchester et al. 2005). From the catalogue, we obtain the pulsar’s spin P , and get

$$\chi_{\text{NS}} = \frac{2\pi cI}{GPM^2}, \quad (10)$$

where c is the velocity of light, G is the universal constant of gravitation, M is the mass of the pulsar (assumed to be $1.4 M_\odot$ here), and I is the moment of inertia of the pulsar given by

$$I = 0.237 M_{\text{NS}} R_{\text{NS}}^2 \left[1 + 4.2 \frac{M_{\text{NS}} \text{ km}}{M_\odot R_{\text{NS}}} + 90 \left(\frac{M_{\text{NS}} \text{ km}}{M_\odot R_{\text{NS}}} \right)^4 \right] \quad (11)$$

(computed from equation 12 of Lattimer & Schutz 2005, with mass $M_{\text{NS}} = 1.4 M_\odot$ and radius $R_{\text{NS}} = 12$ km).

Although most pulsars are expected to spin down significantly due to the loss of rotational energy, with decaying magnetic field at the time of merger (figs 17 and 21 of Chattopadhyay et al. 2021), we take the observed NS spin distribution as an upper limit. The maximum observed spin χ_{NS} is 0.4, with the primary peak at 0.13 and another at about 0.02. The mass distribution for NSs, while dependent on the NS equation of state and the assumed Tolman–Oppenheimer–Volkoff limit for theoretical studies, can also be estimated from pulsar observations (with the inclusion of radio selection effects). Even with

the limited data set due to the difficulty in measuring NS mass, there have been multiple studies to determine the shape and range of the mass distribution of NSs (Antoniadis et al. 2016; Alsing, Silva & Berti 2018; Rocha et al. 2023). For this analysis, we assume the NS mass distribution to be a double Gaussian with a maximum mass of $2.56 M_\odot$, with the bimodal mean peaks at 1.351 and $1.816 M_\odot$ as found and described in details in Rocha et al. (2023) (see table 3). The mass and spin priors for BHs remain uninformed and the NS spins are randomly oriented.

3.3 Models motivated by GW observation of black hole spins

To date, only a small number of NSBH or BHNS binary mergers have been observed (Abbott et al. 2023). This makes it difficult to use the observed properties of these binaries to draw strong inferences about their population properties to be used as prior beliefs when interpreting GW230529. However, during the first three LVK observing runs, close to a hundred BBHs have been observed and the detailed properties of the BH population have been inferred (Abbott et al. 2023). The inferred mass of the more massive component of GW230529 lies outside of the observed BH mass distribution and therefore the existing population mass distribution cannot be used. However, we can use the inferred spin distributions inferred from the BBH population as a proxy for the BH spin distribution

⁴<https://www.atnf.csiro.au/research/pulsar/psrcat/>

in NSBH/BHNS binaries. The inferred spin distribution of BH from observations through GWTC-3 (third Gravitational-Wave Transient Catalog) is shown in fig. 15 of Abbott et al. (2023). The BH spin is modelled through the amplitude χ and orientation $\cos\theta$ of the spin relative to the orbital angular momentum.

The inferred population is given as a set of model distributions, from which an overall average distribution with uncertainty is derived. For the analysis presented here, we obtain the set of distributions, repeat the re-weighting procedure for each distribution, and then average over these draws. The mass distribution of both components and the spin of the NS remain unconstrained.

3.4 Model jointly motivated by observations of radio pulsars and GW binary black holes

As a final model, we combine the astrophysical observations of pulsars from Section 3.2 with those of BHs from Section 3.3 to restrict the properties of both components of the progenitor of GW230529. As a caveat, we caution that these are two very distinct astrophysical populations. Nevertheless, we consider this approach, noting that it can still provide valuable insights into how the choice of priors influences the parameter recovery. We restrict the mass and spin magnitude of the NS from pulsar observations, leaving the spin orientation unconstrained, and we consider the spin magnitude and orientation of the BH from GW observations, leaving the BH mass unconstrained.

4 RESULTS

Fig. 2 shows the inferred mass and spin distributions for the primary and secondary components of GW230529 when we impose astrophysically motivated mass and spin priors, shown in Fig. 1. In all cases, the imposition of astrophysical prior distributions restricts the inferred range of masses and spins, with the biggest impact coming from the use of astrophysical models and the smallest impact from applying the BH spin distribution observed in BBH. For all prior choices, the component masses are more sharply peaked, with reduced support for a close to equal mass, (2.5, 2.0) M_{\odot} , system and preference for an NSBH with a BH mass around 4 M_{\odot} and an NS mass around 1.4 M_{\odot} . Furthermore, we find that the spin distributions narrow, with a preference for low spin magnitudes and reduced support for anti-aligned spins. Interestingly, the results obtained for various astrophysical models are consistent despite these models being used to restrict different subsets of parameters.

The inferred NS and BH masses based on the astrophysical model are sharply peaked at $1.3_{-0.03}^{+0.03}$ and $4.3_{-0.1}^{+0.1}$ M_{\odot} , respectively. This renders the secondary clearly an NS with a mass very compatible with the galactic population and the primary a likely BH in the mass gap. While the object is still in the putative ‘lower mass gap’, it is towards the upper edge; the supernova explosion does not have to be extremely rapid (and hence energetic) to achieve such mass. Interestingly, the restriction on the binary masses does not arise due to the astrophysical mass distribution, but rather the spin distribution. As can be seen in Fig. 1, the NSBH mass distribution for both NS and BH is rather broad, with support from 1.2 to 2.5 M_{\odot} for NS and 2.5 to 6 M_{\odot} for BH. The restriction to (close to) zero spins for both components constrains the mass ratio significantly and, consequently, the component masses. To reiterate, the BHs of the BHNSs are always expected to have zero spin, and the NS, being non-recycled, also effectively zero spins. For NSBHs, pulsar recycling extends the NS spin distribution to larger values, although by the time of merger, it still spins down to $\lesssim 0.1$ –0.2. The BHs of the

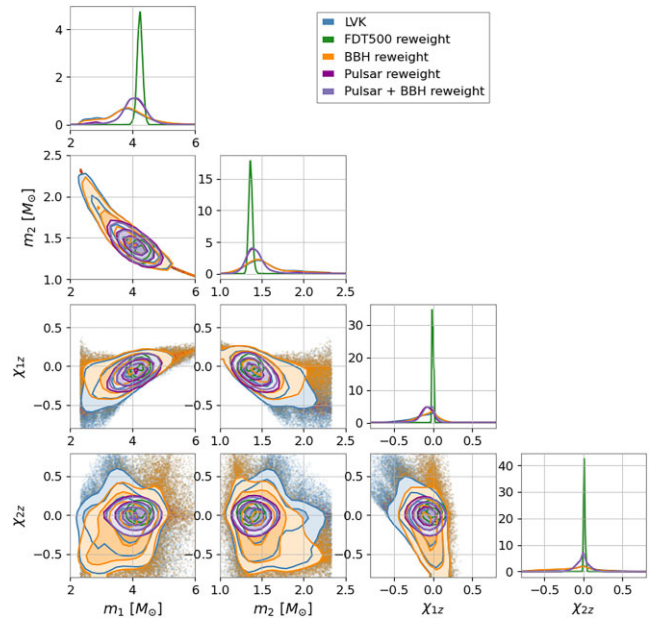


Figure 2. The inferred masses and spin projected along the orbital angular momentum χ_z of the components of GW230529, where the subscripts 1 and 2, respectively, label the heavier and lighter components of the binary, under five different choices of prior. The LVK prior is an uninformative prior, which is flat in redshifted masses and uniform in spin magnitude/orientation; the astrophysical FDT500 prior model is discussed in Section 3.1; the BBH prior uses the χ_{1z} distribution from the observed BBH population; the pulsar prior uses masses and spin magnitudes from observed pulsars and the pulsar + BBH uses both pulsar and BBH observations. Further details of the models are provided in Section 3 and summarized in Table 1. We note that the χ_{1z} prior for the astrophysical models is so sharply peaked close to 0 that we have included samples within $<10^{-2}$ to ensure sufficient prior support for re-weighting.

NSBHs have uncertainty associated with their spins – on one hand, we model the optimistic efficient tidal spin-up model, which gives spins $\chi_z \gtrsim 0.5$ (the FDT500_Q model in Fig. 1); on the other, we assume them to be non-spinning (FDT500). While the tidal spin-up model can be rejected based upon the observed spins, under non-efficient tides we cannot comment definitively on formation order, i.e. NSBH versus BHNS, in this scenario. While NSBHs certainly prefer a more symmetric mass ratio and lower BH masses, the distribution of both sub-systems is sufficiently broad in mass and peaked near zero spins to be fully consistent with the observation of GW230529.

The BBH and pulsar models provide less stringent restrictions on the masses and spins of GW230529. Indeed, the BBH spin prior only restricts the spin of the more massive component and has minimal impact on the masses. The pulsar observations, and combined pulsar and BBH results, do place tighter restrictions on the parameters. These arise due to a combination of NS masses, which peak at 1.35 M_{\odot} but incorporate a high-mass tail, and NS spins that exclude large spin values. The results exclude a binary with equal masses and give a BH with a mass of $3.8_{-0.6}^{+0.5}$ M_{\odot} and an NS with a mass of $1.4_{-0.1}^{+0.2}$ M_{\odot} . The spins are bounded closer to zero, although anti-aligned spins remain possible, particularly for the BH.

The Bayes factors between the different prior assumptions are not the focus of this work and the different models can be partially overlapping and not designed to be compared against each other. However, the correction to the evidence from the analysis in Abac et al. (2024) can be easily computed with the re-weighting approach

(see Payne et al. 2019 for a clear exposition) and we find no significant changes, with the highest effect coming from the astrophysical model with an increase in evidence of $\log_{10} \mathcal{B} \approx 0.5$, comparable to the other effects, such as choice of waveform model, mentioned in Abac et al. (2024).

5 DISCUSSION

This letter re-analyses the GW event GW230529 with a range of astrophysically motivated priors on the masses and spins. This work is complementary to that presented in Abac et al. (2024), where prior distributions derived from the handful of previously observed NSBH observations were used. Here, we have made use of priors derived from population synthesis models of stellar binaries, observations of pulsars in the galaxy, and BBH binaries through GW observations.

The first key point is that the inferred masses and spins of the components of the binary depend critically upon the mass and spin priors used in the analysis and, in particular, the inferred mass distribution is highly dependent upon the spin prior. The fact that the distributions are so reliant on the prior demonstrates that the uncertainties in the observations for this system are large, due to the relatively low SNR of the event. Therefore, we cannot draw strong conclusions about the origin of this event.

However, we also note that under three distinct sets of astrophysically well-motivated choices of mass and/or spin priors, we arrive at a similar conclusion: that the preferred progenitor of GW230529 was a binary composed of an NS and a BH, where the NS is entirely consistent with the observed galactic population and the BH lies at the upper end of the purported ‘lower mass gap’ between 2.5 and 5 M_{\odot} .

Even with the most optimistic (i.e. broadest) observationally motivated spin priors – BBH (non-zero spin distribution from GW catalogue GWTC-3) and the millisecond pulsar spins (not accounting for pulsar spin-down at merger), our results are unaltered. We also conclude that while we cannot rule out any of the astrophysical models described in Section 3.1, or say with certainty that the NS was formed before the BH, we can most definitely rule out the tidal spin-up of the BH, hence rendering the lack of observed electromagnetic counterpart unsurprising (Barbieri et al. 2020). Higher SNR, multiple-detector observation (for better sky localization), and an order-of-magnitude closer events in future GW observing runs will provide improved ability to accurately measure the binary parameters, and increase the chance of observing electromagnetic counterparts to similar observations in the future. The observation of low-mass, high-spin BHs will provide evidence of tidal spin-up and also provide a greater chance of observing a counterpart.

ACKNOWLEDGEMENTS

We thank Vivek Venkatraman Krishnan, Mark Hannam, and Alexandre Göttel for the useful discussions. DC, FA, SF, and VR were supported by the UK’s Science and Technology Facilities Council grant ST/V005618/1. SA-S was funded by UKRI Centre for Doctoral Training in Artificial Intelligence, Machine Learning & Advanced Computing. The authors are grateful for computational resources provided by Cardiff University, which are supported by STFC grants ST/I006285/1 and ST/V005618/1. The astrophysical model grid was run in the OzSTAR high-performance supercomputer at Swinburne University of Technology. OzSTAR is funded by Swinburne University of Technology and the National Collaborative Research Infrastructure Strategy (NCRIS). This research has made use of data or software obtained from the Gravitational Wave

Open Science Center (gwosc.org), a service of the LIGO Scientific Collaboration, the Virgo Collaboration, and KAGRA. This material is based upon work supported by NSF’s LIGO Laboratory, which is a major facility fully funded by the National Science Foundation, as well as the Science and Technology Facilities Council (STFC) of the United Kingdom, the Max-Planck-Society (MPS), and the State of Niedersachsen/Germany for support of the construction of Advanced LIGO and construction and operation of the GEO600 detector. Additional support for Advanced LIGO was provided by the Australian Research Council. Virgo is funded, through the European Gravitational Observatory (EGO), the French Centre National de Recherche Scientifique (CNRS), the Italian Istituto Nazionale di Fisica Nucleare (INFN), and the Dutch Nikhef, with contributions by institutions from Belgium, Germany, Greece, Hungary, Ireland, Japan, Monaco, Poland, Portugal, and Spain. KAGRA is supported by the Ministry of Education, Culture, Sports, Science and Technology (MEXT), Japan Society for the Promotion of Science (JSPS) in Japan; National Research Foundation (NRF) and the Ministry of Science and ICT (MSIT) in Korea; and Academia Sinica (AS) and National Science and Technology Council (NSTC) in Taiwan.

DATA AVAILABILITY

The data utilized for this work will be freely available upon reasonable request to the corresponding author.

REFERENCES

- Abac A. G. et al., 2024, *ApJ*, 970, L34
 Abbott R. et al., 2021, *ApJ*, 915, L5
 Abbott R. et al., 2023, *Phys. Rev. X*, 13, 011048
 Alsing J., Silva H. O., Berti E., 2018, *MNRAS*, 478, 1377
 Antoniadis J., Tauris T. M., Ozel F., Barr E., Champion D. J., Freire P. C. C., 2016, preprint ([arXiv:1605.01665](https://arxiv.org/abs/1605.01665))
 Bailyn C. D., Jain R. K., Coppi P., Orosz J. A., 1998, *ApJ*, 499, 367
 Barbieri C., Salafia O. S., Perego A., Colpi M., Ghirlanda G., 2020, *Eur. Phys. J. A*, 56, 8
 Barr E. D. et al., 2024, *Science*, 383, 275
 Bavera S. S. et al., 2020, *A&A*, 635, A97
 Belczynski K., Taam R. E., Kalogera V., Rasio F. A., Bulik T., 2007, *ApJ*, 662, 504
 Belczynski K., Wiktorowicz G., Fryer C. L., Holz D. E., Kalogera V., 2012, *ApJ*, 757, 91
 Blanchet L., 2006, *Living Rev. Relativ.*, 9, 4
 Broekgaarden F. S. et al., 2021, *MNRAS*, 508, 5028
 Chandra K., Gupta I., Gamba R., Kashyap R., Chattopadhyay D., Gonzalez A., Bernuzzi S., Sathyaprakash B. S., 2024, preprint ([arXiv:2405.03841](https://arxiv.org/abs/2405.03841))
 Chattopadhyay D., Stevenson S., Hurley J. R., Rossi L. J., Flynn C., 2020, *MNRAS*, 494, 1587
 Chattopadhyay D., Stevenson S., Hurley J. R., Bailes M., Broekgaarden F., 2021, *MNRAS*, 504, 3682
 Chattopadhyay D., Stevenson S., Broekgaarden F., Antonini F., Belczynski K., 2022, *MNRAS*, 513, 5780
 Cutler C., Flanagan E. E., 1994, *Phys. Rev. D*, 49, 2658
 Elvira V., Martino L., Robert C. P., 2018, *Int. Stat. Rev.*, 90, 525
 Farr W. M., Sravan N., Cantrell A., Kreidberg L., Bailyn C. D., Mandel I., Kalogera V., 2011, *ApJ*, 741, 103
 Fryer C. L., Belczynski K., Wiktorowicz G., Dominik M., Kalogera V., Holz D. E., 2012, *ApJ*, 749, 91
 Goertzel G., United States Atomic Energy Commission, Oak Ridge National Laboratory, 1950, Quota Sampling and Importance Functions in Stochastic Solution of Particle Problems. AECD, U.S. Atomic Energy Commission, Technical Information Division, United States of America, Accessed 1 November 2024, <https://books.google.co.uk/books?id=Su1EYGagoAC>

- Hannam M., Brown D. A., Fairhurst S., Fryer C. L., Harry I. W., 2013, *ApJ*, 766, L14
- Hurley J. R., Pols O. R., Tout C. A., 2000, *MNRAS*, 315, 543
- Hurley J. R., Tout C. A., Pols O. R., 2002, *MNRAS*, 329, 897
- Ivanova N. et al., 2013, *A&AR*, 21, 59
- Kish L., 1995, *Survey Sampling*, 3rd edn. Wiley-Interscience, Oxford, England
- Lattimer J. M., Schutz B. F., 2005, *ApJ*, 629, 979
- LIGO Scientific Collaboration, Virgo Collaboration, KAGRA Collaboration, 2024, Observation of Gravitational Waves from the Coalescence of a 2.5–4.5 Msun Compact Object and a Neutron Star – Data Release. Dataset, Zenodo, <https://doi.org/10.5281/zenodo.10845779>
- Liu J. S., 2004, *Monte Carlo Strategies in Scientific Computing*. Springer, New York
- Manchester R. N., Hobbs G. B., Teoh A., Hobbs M., 2005, *AJ*, 129, 1993
- Martineau T., Foucart F., Scheel M., Duez M., Kidder L., Pfeiffer H., 2024, preprint ([arXiv:2405.06819](https://arxiv.org/abs/2405.06819))
- Olejak A., Fryer C. L., Belczynski K., Baibhav V., 2022, *MNRAS*, 516, 2252
- O’Shaughnessy R., Kim C., Kalogera V., Belczynski K., 2008, *ApJ*, 672, 479
- Özel F., Psaltis D., Narayan R., McClintock J. E., 2010, *ApJ*, 725, 1918
- Payne E., Talbot C., Thrane E., 2019, *Phys. Rev. D*, 100, 123017
- Qin Y., Fragos T., Meynet G., Andrews J., Sørensen M., Song H. F., 2018, *A&A*, 616, A28
- Riley J. et al., 2022, *ApJS*, 258, 34
- Robert C. P., Casella G., 2004, *Monte Carlo Statistical Methods*, 2nd edn. Springer, New York
- Rocha L. S., Horvath J. E., de Sá L. M., Chinen G. Y., Barão L. G., de Avellar M. G. B., 2023, *Universe*, 10, 3
- Ronchini S. et al., 2024, *ApJ*, 970, L20
- Siegel J. C. et al., 2023, *ApJ*, 954, 212
- Stevenson S., Sampson M., Powell J., Vigna-Gómez A., Neijssel C. J., Szécsi D., Mandel I., 2019, *ApJ*, 882, 121
- Veitch J. et al., 2015, *Phys. Rev. D*, 91, 042003
- Xu X.-J., Li X.-D., 2010, *ApJ*, 716, 114
- Ye C. S., Fong W.-f., Kremer K., Rodriguez C. L., Chatterjee S., Fragione G., Rasio F. A., 2020, *ApJ*, 888, L10
- Zevin M., Spera M., Berry C. P. L., Kalogera V., 2020, *ApJ*, 899, L1
- Zhu J.-P., Hu R.-C., Kang Y., Zhang B., Tong H., Shao L., Qin Y., 2024, *ApJ*, 974, 211

This paper has been typeset from a $\text{\TeX}/\text{\LaTeX}$ file prepared by the author.